Journal of Hunan University

(Natural Sciences)

Vol. 52 No. 11

November 2025

Available online at

https://jonuns.com

Open Access Article

https://doi.org/10.55463/issn.1674-2974.52.11.6

PHiL implementation of a real-time EMS for a multilevel converter powered by ultracapacitors

Javier Eduardo Pereda-Torres[1], Walter Naranjo-Lourido[2], Javier Eduardo Martinez-Baquero[3*]

[1]Department of Electrical Engineering, Pontificia Universidad Católica de Chile, Santiago, Chile,

[2,3]Professor of Engineering School, Faculty of Basic Sciences and Engineering, Universidad de los Llanos, Villavicencio, Colombia,

* Corresponding author: jmartinez@unillanos.edu.co

Article history:
Received: October 19, 2025
Revised: November 26, 2025
Accepted: December 11, 2025
Published: December 30, 2025

Abstract: This paper presents a real-time energy management system (EMS) for an electric powertrain, tested using a Power Hardware-in-the-Loop (PHIL) platform. The system is built around a two-layer multilevel inverter (MLI) with ultracapacitors (UCaps) as distributed energy storage, capable of producing up to 11 line-to-line voltage levels. To manage energy flow and maintain the required 1:3 voltage ratio between the main and auxiliary UCap banks, a predictive vector-selection strategy is implemented within a space vector modulation with nonlinear compensation (SVM-NLC) scheme. Experimental results show that SVM-NLC achieves a higher inverter efficiency of 91.71% compared to 90.55% for conventional SVPWM, while keeping UCap voltage tracking within 5% error. The SVPWM reference also demonstrates a low output current total harmonic distortion (THD) of 0.64%, illustrating the benefits of the multilevel design. Under the testbed's 100 A current limit, the PMSM delivers a maximum torque of 9.89 Nm, allowing accurate reproduction of a scaled ECE15 driving cycle. Overall, the proposed EMS efficiently distributes energy during both traction and regenerative braking, ensuring stable real-time operation and high energy recovery performance.

Keywords: Electric Vehicle, Energy Management System, Hardware-In-the-Loop, Multilevel Inverter, Ultracapacitors.

基於超級電容器供電的多級轉換器之即時電能管理系統的 PHiL 實現

摘要： 本文提出了一种用于电动动力系统的实时能量管理系统（EMS），并在功率硬件在环（PHIL）平台上进行了测试。该系统基于双层多电平逆变器（MLI），采用超电容器（UCaps）作为分布式储能，能够产生多达 11 个线间电压等级。为管理能量流动并保持主、辅超电容组之间 1:3 的电压比，系统采用了基于预测向量选择的空间矢量调制非线性补偿（SVM-NLC）策略。实验结果显示，SVM-NLC 实现的逆变器效率为 91.71%，高于传统 SVPWM 的 90.55%，同时保持超电容电压跟踪误差小于 5%。SVPWM 参考方案的输出电流总谐波失真（THD）为 0.64%，显示了多电平设计在谐波抑制方面的优势。在测试台 100 A 电流限制下，永磁同步电机（PMSM）能够输出最大扭矩 9.89 Nm，从而准确再现缩放的 ECE15 驾驶循环。总体而言，该 EMS 在牵引和再生制动过程中有效分配能量，确保实时运行稳定，并实现高能量回收性能。

关键词：電動車輛、能源管理系統、硬體在迴路測試、多層次逆變器、超級電容器。

1. Introduction

EMSs are fundamental in several aspects of E.V.s, from the power distribution on the charge spots to the energy powertrain control for extending the E.V. range. Different [1–4] initially focus on answering the dynamic energy demand of the E.V.s, especially from the energy distribution system. In [2] is used Modelica joined to an agent's software to estimate the energy demand is unforeseeable by traditional analysis. Also, in [1] is established a method for distributing and optimizing the energy demand on the buildings, according to E.V. requirements.

According [3-4] the primary objectives of an EMS in E.V.s are to maximize powertrain energy usage hile in driving mode and recover all potential energy from regenerative braking. The electric powertrain's storage systems, however, put a cap on how well the EMS performs. Different EMS approaches have been developed according to various studies [5–9]. These approaches had excellent results in extending driving autonomy and substantially lowering switching and conduction inverter losses. In [3],[10–12], another EMS for E.V.s with HES is created after analyzing and developing the best size and power distribution between energy sources. As a result, a range increasing of 8.9% using neuronal networks reported in [3], extended the battery life in a 60% [10], and energy savings of up to 7.8% [12].

Some technical advantages are an improved voltage THD, a lower distortion on the current signal, a low switching frequency for reducing the switching losses, and some modulation techniques that can eliminate some harmonic selected. Studies performed by [13-17] have demonstrated different technical advantages of MLI, which allow extending the driving autonomy of the E.V. For this reason, the MLI has received more attention due to its high energy performance over conventional inverters.

The main manuscript contributions are: (a) a real-timeimplementation of an electric powertrain through the use of a PHiL, (b) The proposed EMS guarantees the inverter stability under different operational conditions; (c) improving the energy performance of the powertrain system when is used the high specific power of the UCaps. This paper proposes an energy management system of an electric powertrain implemented in a testbed using a Power hardware-in-theloop. This real-time powertrain implementation was inspired by a conventional multilevel inverter of two layers that uses ultracapacitors as an energy storage system. Additionally, this manuscript proposes a flexible inverter that redirects the bidirectional energy flux inside the powertrain according to EMS decisions.

The manuscript's purpose is to design, implement, and verify an EMS for an MLI-powered electric powertrain. The analytical paradigm for energy management is thus developed and described in this manuscript. After that, the suggested approach is put into practice in a testbed with a HiL configuration to verify the energy management strategy.

The paper's organization is detailed as follows. Chapter 2 explains the proposed MLI topology used in an E.V., including the considered modulations and its flexibility to redirect the energy flux inside the powertrain and explains the proposed EMS's design and implementation over a whole powertrain using a HiL component. Afterward, chapter 3, reports and explains the results of the EMS inside the electric powertrain. Finally, the manuscript presents the conclusion.

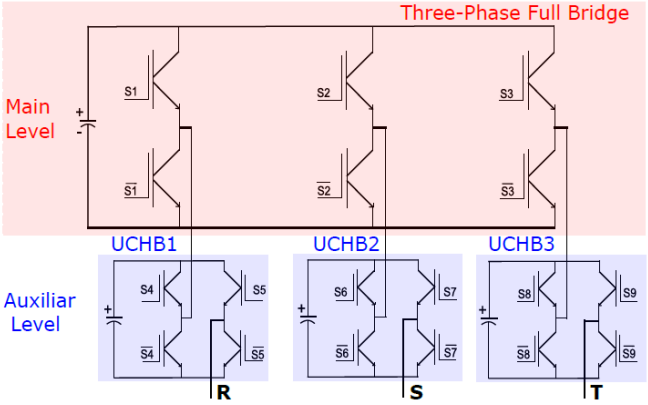

Figure 1. MLI Proposed Topology with UCaps Energy Storage (Source: developed by the authors)

2. Methodology

This section explains the proposed topology, the possible modulations considered for its use, the dynamic modeling of the E.V., and the energy losses performed to the electric powertrain.

2.1. Multilevel Inverter Topology

According to Figure 1, the suggested MLI topology consists of a main level (with a three-phase full-bridge) and an auxiliary level with three half-bridges and floating UCaps, one on each leg. UCaps, a special form of energy storage, are distributed across both layers in this topology. The MLI can turn off any inverter level necessary to regulate the flow of engine energy.

This flexible MLI topology controls the bidirectional energy flux of the UCaps according to driving requirements under three modes: driving mode, braking mode, and transfer energy mode. The topology can be transferred from the main to the auxiliary sources for the first mode. Simultaneously, the proposed topology can give energy to the electric motor. Similarly, braking mode can be a potential early recovery, with a significant portion of the braking energy using the UCaps and redirecting to the battery. As a result, energy recuperation is more effective thanks to the UCaps' high specific power. For the transfer energy option, energy can be transferred between inverter levels. As a result, the EMS has authority over the energy moving from the battery to the UCaps or vice versa. This mode is feasible by choosing redundant vectors without affecting the motor current.

On the other hand, this MLI topology can generate up to 11 line-to-line voltage levels with a THD lower than 10%, according to the IGBT switching. Clarke transformation is used to select the adequate switching vector, a three-phase trigger vector, over a 2D space. The Clarke transformation is defined in (1). In Figure 2, all possible trigger vectors are plotted in the domain 2D of Clarke transformation for its posterior selection. The distribution of the space voltage vector changes because of variations in the UCaps voltage. These vector space changes are directly related to the main and auxiliary radius. So, if the auxiliary receives energy from the main, the auxiliary radius is incremented. Meanwhile, the main radius remains practically unchanged due to a higher capacitance.

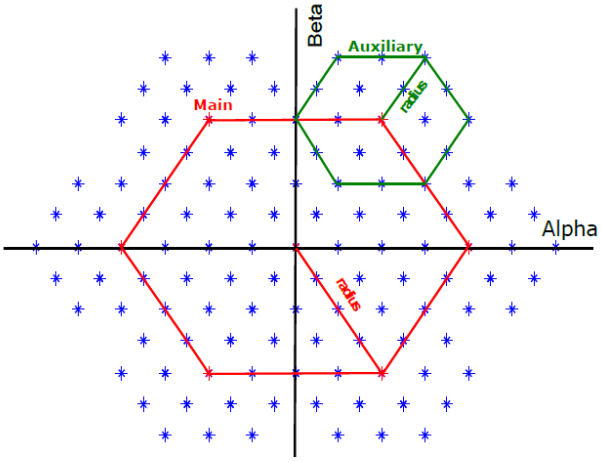

Figure 2. Topology switching vectors represented on alpha-beta space (Source: developed by the authors)

$$\begin{bmatrix} V_\alpha \\ V_\beta \end{bmatrix} = \begin{bmatrix} 1 & -1/2 & -1/2 \\ 0 & \frac{\sqrt{3}}{2} & -\frac{\sqrt{3}}{2} \end{bmatrix} \begin{bmatrix} V_a \\ V_b \\ V_c \end{bmatrix} \quad (1)$$

In order to prevent over-modulation, the vector election method requires a reference, such as a circular reference, to be contained within the vector's outer hexagon. The chosen method is also influenced by the electrical frequency and voltage needed for the inverter output. The counterclockwise rotational speed Ω [rad/s] serves as the electrical frequency guide. Therefore, an SVM-NLC and an SVPWM are assessed for this scenario's trigger vector selection.

2.2. Evaluated Modulation

In this section, both modulations (NLC and SVPWM) are evaluated. Initially, the modulations are briefly explained, and then energy is evaluated. For this, an energy losses analysis of the proposed topology is performed utilizing a previous methodology established by the authors in [18]. The previous methodology analyzes the switching and conduction losses of the proposed topology in front of a driving cycle. Similarly, this work evaluates the proposed methodology using the ECE15 driving cycle.

1) Space Vector Modulation SVM with NLC: This modulation determines the voltage and electrical frequency output of the inverter, which finds the trigger vector closest to a reference vector. This control also allows selecting one of several redundant vectors for maintaining the voltage ratio between the main and secondary levels and balancing the UCaps of each phase. The switching frequency of an NLC is smaller in comparison to other modulations. As an outcome,

reduced losses are provided by the NLC due to switching frequency, but conduction losses must be assessed.

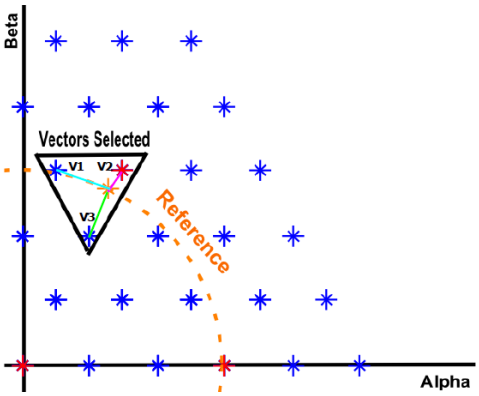

Figure 3. Selection of SVPWM vectors (Source: developed by the authors)

2) Space Vector Pulse Width Modulation SVPWM: The SVPWM reaches any point inside the Clarke space transformation due to the linear vector combination of the three adjacent vectors. Figure 3. The vectors are selected according to their proximity to the reference for subsequent switching between them. These adjacent vectors must always enclose the reference inside a triangle. Otherwise, the SVPWM cannot generate an equivalent vector to the reference. As additional information, it is essential to highlight some redundant vectors inside the SVPWM used to perform the EMS control.

For the switching PWM among vectors, different switching times T_0, T_1, T_2, and T_3 are determined according to their proximity to the reference for controlling the resulting vector modulation. In (2) are determined the switching times $T_{0\text{-}3}$ according to the relative distance $D_{1\text{-}3}$, between trigger and reference vectors.

$$Tsw(s) \begin{cases} T_0 = \frac{D_1}{D_{Total}} T_s/2 \\ T_1 = \frac{D_2}{D_{Toral}} T_s \\ T_2 = \frac{D_3}{D_{Total}} T_s \\ T_3 = \frac{D_1}{D_{Total}} T_s/2 \end{cases} \quad (2)$$

3) Modeling of the electric powertrain: This section models the E.V. dynamics through a low-order longitudinal model. The proposed model predicts the vehicle behavior for the driving requirements. In this case, it is considered a front traction vehicle. Using the Newton laws, this dynamic model is obtained from the analysis of Figure 4. Thus, it is possible to determine the (3), (4), and (5). Additionally, using a torque summation equation around the contact point of the rear tire and a pre-established driving cycle is posible to deduct the torque requirements of the electric motor. From (6) and neglecting any tire slip, the resistive torque on the front wheel is shown in (7). The engine torque is obtained considering the mechanical reductions from the motor to the traction wheel (8). This resistive torque calculation is essential input data for the EMS simulation.

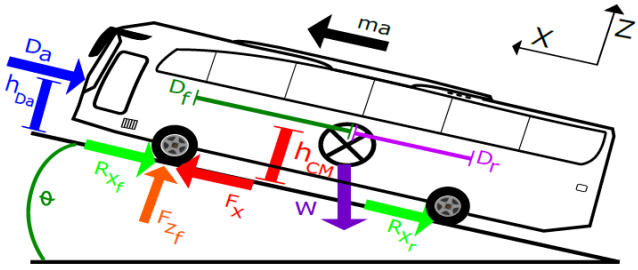

Figure 4. Low-order Longitudinal Model (Source: developed by the authors)

$$F_x - R_x - D_a - F_g = m_{eq}a \quad (3)$$

$$R_x = F_r w \quad (4)$$

$$D_a = 0.5\rho A C_d S^2 \quad (5)$$

$$F_{Zf} = \frac{-D_a h_{Da} - w h_{cm} sin\theta + w D_r cos\theta + m_{eq} a h_{cm}}{D_f + D_r} \quad (6)$$

$$T_{wres} = R_x r + D_a(h_{D_a} - r) + wcos\theta D_f + wsin\theta\,(h_{cm} - r) \quad (7)$$

$$T_{e_{res}} = T_{w_{res}}/N_{tf}\eta_{tf} \quad (8)$$

4) Energy losses: The prior analysis was completed using the suggested online methodology in [18] to determine an appropriate modulation for the testbed. The authors of this manuscript put forth and showed the methodology used at the IECON15 conference. The load equation model and the inverter efficiency suggested in (9) and (10) were both required for this study. In order to execute the simulation, the model also needs the PMSM and vehicle characteristics listed in Table 1 and Table 2.

$$Te = (meqdS\,dt + Frw + Da)r\,Ntf\,tf \quad (9)$$

$$\eta_{inv}[\%] = (1 - \frac{E_{Cond} + E_{sw}}{\int V_{dc} I_{dc} dt})\,100\% \quad (10)$$

The simulation was performed using the ECE15 driving cycle using both modulations. As a result, the SVM-NLC has an efficiency of 91.71 % compared to 90.55 % of the SVPWM. However, the SVPWM presents a better THD current (0.64 %) than the SVM-NLC.

On the other hand, selecting an adequate modulation is critical to consider the maximum switching frequency of the inverter. For ECE15 experimental reproduction, the máximum electrical frequency of the inverter is lower than 160 Hz for a Ntf= 7. Thus, for the SVPWM case, the switching frequency is limited by the IGBT performance. The SVPWM simulation was performed with an IGBT operation frequency of 20 kHz. Consequently, the HiL control must be 10x faster than

the operating frequency to prevent latencies and guarantee a real-time response.

This work decided to implement the proposed EMS using SVM-NLC due to its higher energy performance and better time slots for taking control decisions.

Table 1. Electric Motor Paraeters

Parameters	Value
Nominal Power (kW)	20
Voltage (VAC)	65,6 VAC
Current (A)	255 ARMS
Speed (rpm)	6000
Torque (Nm)	35
Voltage constant (V/1000rpm)	8.87
Torque constant (Nm/A)	0.14
Number of Poles	8
Frequency (Hz)	400
Resistance (Ru–v)	0.0049 Ohm
Inductance (Lu–v)	0.053333 mH
Inertia J (kg·cm²)	58.6

Table 2. Vehicle Parameters

Parameters	Value
Rolling Coefficient (Fr)	0.0117
Drag Coefficient (Cd)	0.53
Cross section Area (A)	8.8 m²
Air density (ρ)	1 kg/m³
Equivalent mass (mequ)	18,000 kg
Total Powertrain Efficiency (η)	0.9

2.3. Energy Management System (EMS)

In this paper, the EMS aims to control the UCaps energy fluxinside the powertrain under different driving conditions. Two driving mode conditions are defined to implement the EMS strategy. The first condition is the traction mode, where the ESS gives the wheel energy to overcome resistive forces. As the second condition, we found the regenerative mode, where the PMSM generates a Back-EMF due to vehicle inertia and the vehicle's kinetic energy.

A basic overview of the suggested EMS is shown in Figure 5, where the EMS depends entirely on the function mode. For instance, the real-time control handles the modulation finding in traction mode and chooses the best redundant vector to correct and maintain the voltage ratio between levels. As a result, it is feasible to ensure that the main level provides the majority of the energy, cutting down on losses brought on by its low switching frequency. Instead, when using regenerative braking, the EMS keeps track of the energy stored in each level and redirects it first to the primary level and then to the auxiliary level. Energy would be split between mechanical and regenerative braking in he regenerative mode without compromising the car's safety.

The proposed inverter topology permits to perform control over the energy fluxes inside the powertrain. Under this perspective, the energy management in the UCaps is directly related to its voltages. Thus, implementing an EMS is necessary to establish a UCHB auxiliary voltage control for traction and regenerative mode. This UCHB voltage control can be established through the SVM-NLC choosing adequate vectors that permit controlling and balancing the UCaps voltages. So, using and evaluating all redundant vectors closest to the reference, it is possible to establish a predictive voltaje control for the UCHB. For the traction mode, a minimum cost function is determined for establishing the predictive voltaje control, as shown in (11) and (12).

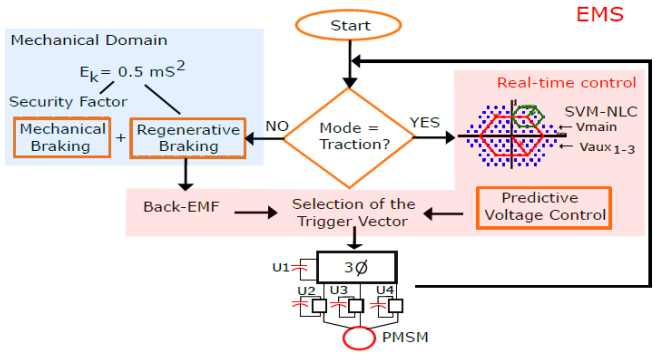

Figure 5. General overview of the proposed EMS (Source: developed by the authors)

$$J(k) = \sum_{j=1}^{M} \left(v_{cap}{}^{*} - v_{cap-j}\left(t + T_S \,|\, k\right) \right)^2 \quad (11)$$

$$v_{cap-j}(t + T_S \,|\, k) = \frac{T_S}{C_j}\, \vec{i}\vec{S}j(k) + v_{cap-j}\,(t) \quad (12)$$

where,

$v^{*}_{cap} = v_{main} = 3$

$\sim i = [i_a\ i_b\ i_c]$

The predictive model permits determining the effects over the UCaps voltages when a selected trigger vector is applied for each sample time. The voltage ratio between the main and auxiliary levels must always be the same. In this case, the voltage ratio is 1:3. It is possible to guarantee a similar trigger vector distribution inside the alpha-beta space across the driving cycle. An auxiliary formula establishes the voltaje ratio error, shown in (13).

$$\epsilon_{ratio} = \sum_{j=1}^{1} \left(\frac{v_{main}}{3} - v_{cap-j} \right)^2 \quad (13)$$

On the other hand, the energy capacity for each level is determined in the regenerative mode. Thus, the EMF will determine which level still works during the back-EMF to recover the kinetic energy.

The inrush capacitor current was not limited in the suggested energy strategy since the responsibility for restricting the load current when the electric vehicle (EV) powered by ultracapacitors arrives at the station lies with the charger. The Multi-Level Inverter (MLI) topology used in this system requires a 1:3 voltage ratio between the main and auxiliary levels, which can be provided by the charger. Consequently, the limitation of inrush current is beyond the scope of this work. However, it is crucial to establish current limits to ensure safe operating conditions during the charging process. By appropriately setting these limits, the charger can effectively mitigate the impact of inrush current and prevent excessive stress on the system. Moreover, the inherent characteristics of ultracapacitors allow them to efficiently handle high currents, thereby minimizing the effects of inrush current.

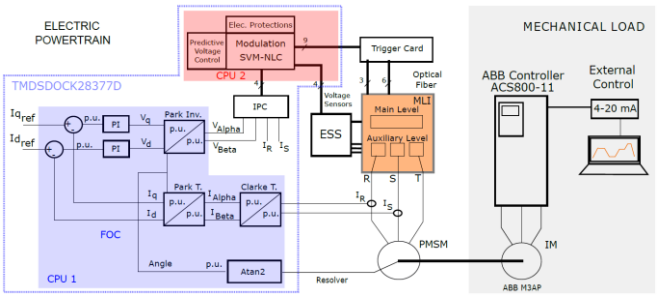

Figure 6. Implementation of the proposed MLI (Source: developed by the authors)

Furthermore, the proposed energy strategy primarily focuses on fulfilling power requirements during vehicle movement, specifically when the EV is in motion. Consequently, the energy stored in the ultracapacitors generally decreases over time, except during regenerative braking, where a reverse flow of energy is generated. However, this regenerative energy is lower than the consumed energy. As a result, the system is incapable of generating a current peak when the vehicle decelerates normally at a rate below 1.5 m/s^2, as per the vehicle dynamics described by Gillespie.

Before proceeding with the hardware implementation, extensive simulations were conducted using Matlab® to examine a range of test conditions. These evaluations check the capacitors voltage balancing inside the MLI during the operation of electric motor. The simulations were performed with the ECE15 standard test drive, a widely adopted method for assessing energy consumption and emissions. The primary objective was to calculate and simulate various dynamic parameters, including voltages, currents, and trigger vectors, across different operational points. Importantly, these simulations proceeded without encountering any stability issues.

Throughout the simulations, the Energy Management System (EMS) consistently predicted the most suitable trigger vector to maintain a 1:3 voltage relationship between the main and auxiliary levels. This proactive approach not only ensured the system's stability but also facilitated efficient energy management during the entire simulation process. Additionally, to validate the effectiveness of the proposed operational conditions, online verification was performed using the Power Hardware-in-the-Loop (PHiL) testbed.

1) Proposed methodology for the EMS implementation: This modulation determines the voltage and electricalIn this subsection, a whole electric powertrain model is simulated and implemented. The proposed MLI and the full implementation are shown in Figure 6. The model considers the energy chain from the ESS to the electric motor inside the electric powertrain. For this case, a PMSM is used as the mechanical actuator.

A FOC is selected as the control method due to its technical advantages. The FOC controls the stator currents represented by a vector in a *dq*0 coordinate system invariant over time. Initially, this technique uncouples the stator flux's torque control, allowing the torque regulates the speed through Iq. The FOC technique has a high performance in the fast dynamics of the electric motor. Additionally, the FOC algorithm has a fast execution, which is ideal for real-time controllers.

An MCU-DSP (TMDSDOCK28377D) of T.I. implements the FOC and the SVM-NLC. This MCU-DSP was chosen due to its low-cost and dual-core architecture capable to build the EMS. Both independent cores are used to distribute the computational load as shown in Table 3.

FOC Implementation is in Code Composer Studio CCS (Eclipse); this technique is done by programming in C + +, occupying a high-priority periodic interruption of DSP (13 kHz) for execution. During execution, they executed several macros: CLARKE_MACRO converts a three-phase in a bi-phase current; PARK_MACRO calculates the Iq and Id stationary currents, which are related to the rotor shaft; IPARK_MACRO to transform again Vd, Vq to alpha-beta space; and of course the P.I. for adjusting the control response using PI_MACRO.

Table 3. Distribution of the computational load in F28377D

CPU 1	CPU 2
UCaps voltage readings	Build alpha-beta space
Current readings	Trigger vector selection
Resolver reading & angle calculation	High-level UCaps voltage control
Signals filtering	Security algorithm to prevent I & V spikes
FOC implementation	Receiving parameters by IPC
Sending parameters by IPC	Parameters conversion to Full-scale

In the first core, a FOC sense the currents of R and S phases and the motor position to adjust the modulation. The FOC is shown in Figure 6 utilizing different space transformations such as Clarke and Park (stationary or rotating frames) to determine the trigger vectors for the SVM-NLC. In this case, an MTPA technique is used as frequency and amplitude modulation for torque control of the PMSM. So, the I_{dref} current is fixed to zero, and I_{qref} current is adjusted dynamically by the torque requirements of the driving cycle. As a result of this FOC, two signals, V_{Alpha} and V_{Beta}, are delivered to the IPC, which communicates both cores.

The second core receives four signals (V_{Alpha}, V_{Beta}, I_R, I_S) to build the alpha-beta space and control the powertrain energy through a predictive vector selection. Also, this core has functions of electric safety. All the time, the cores supervise the dv/dt and di/dt occasioned during the switching transition, and just in the case that the safety limits exceed the trigger signal turns off, MLI. Afterward, the trigger card processed the signals, transforming the electrical to an optical signal, preventing false triggering of IGBTs. Thus, the MLI changes its behavior and adjusts its output to give adequate motor torque control.

On the other side, the mechanical load is implemented with an industrial motor controller of 4 quadrants (ABB ACS800-11), which controls a 3 kW I.M. (ABB M3AP). This device is controlled through an external laptop that provides a 4 to 20 mA signal according to the load torque required by the driving cycle. The EMS applied inside the powertrain is evaluated using an ECE15 standard driving cycle designed for urban driving. This ECE15 driving cycle is a single unit of the NEDC reported in the literature.

2) Testbed implementation: Before it describes the implementation process; it is necessary to define the electric motor parameters as the characteristic vehicle parameters required to evaluate the proposed EMS. All electric parameters are shown in Table 1, and the vehicle parameters in Table 2. Additionally, all P.I. of FOC control was adjusted for the inverter configuration.

Now for the testbed implementation, different PCBs were performed to implement the proposed MLI shown in Figure 7, taking into account the vehicle and electrical requirements. Four kinds of PCBs were designed: a current and voltage sensor card, the main trigger card, an auxiliary trigger card, and an optical trigger card, which are shown in Figure 8. The current and voltage sensor card is charged with conditioning and filtering all MCU signals to 3.3 Vdc. Also, the main and auxiliary trigger card manages the switching of the IGBTs and simultaneously generates the dead time to prevent a short circuit in each leg. Additionally, these cards receive an optical signal to avoid false triggers by EMI. Finally, the optical trigger card performs the signal conditioning between the MCU and the trigger cards. All the testbed electrical components and requirements are defined in Table 4.

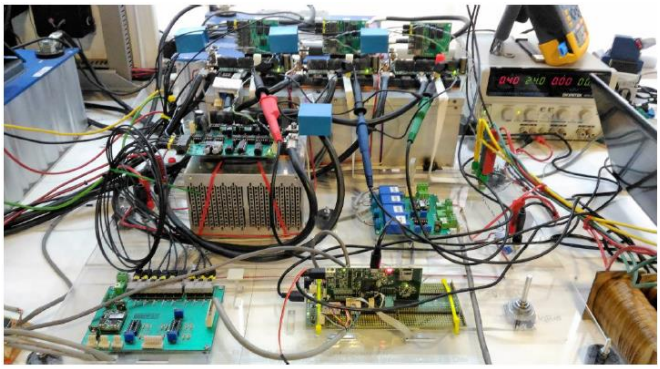

Figure 7. Implementation of the proposed MLI (Source: developed by the authors)

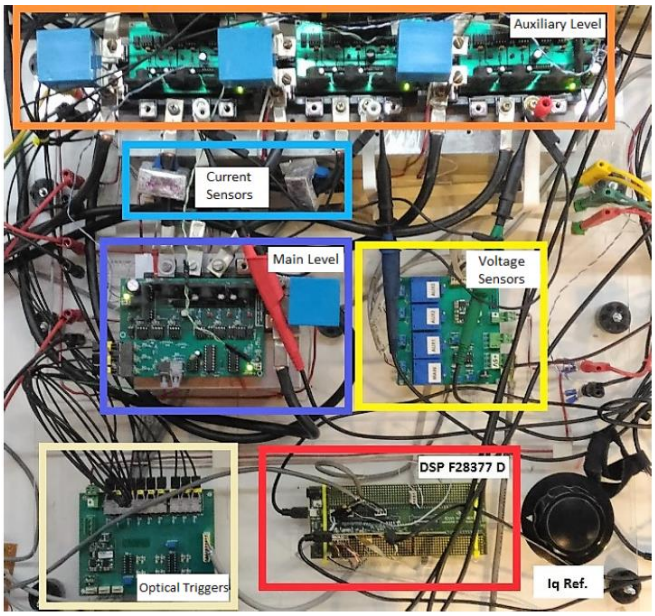

Figure 8. MLI diagram block scheme (Source: developed by the authors)

Table 4. Requirements for Testbed Implementation

UCaps Characteristics	5 Maxwell BMOD0165 P048
Capacitance (Main / Auxs)	330 /165 F @48 V
MLI Characteristics	4 Intellimod PM100CLA060
Voltage ration (Vmain / Vaux)	1:3
Main voltage	33 V
Auxiliary voltage	11 V
Maximum power	100 A @ 1200 V (120 kW)
Work power inverter	100 A @ 1200 V (120 kW)
Real-time Processor	TI TMDSDOCK28377D
MCU-DSP Frequency	200 MHz
Cores	2
FOC frequency	13 KHz
Sensors	
Resolver AM256 frequency @ Max. RPM	1 KHz
Work resolver frequency @1750 RPM	291 Hz
Voltage Sensor (4 Units)	LV-20P
Current Sensor (2 Units)	HAS 100-S

The MLI was built and installed in acrylic 8 mm as a modular prototype with a power capacity of 120 kW. The wiring between the main and auxiliary levels has a cable 2/0 to handle currents up to 150 A. The mechanical coupling was built in steel and aluminum. An elastic coupling to prevent motor blocking and shaft misalignment was used to join the shafts of both motors. The load IM has 3 kW (19,7 nm) @ 1450 rpm. Meanwhile, the PMSM was used as a traction motor at 22 kW (30 Nm) @ 6000 rpm. For the different characteristics of the motors, adequate torque and current control must prevent mechanical damage.

The electric powertrain and the proposed MLI were designed and built, as shown in Figure 9, in the Power and Energy Converter Laboratory PECLab of the department of engineering of the Pontificia Universidad Católica de Chile.

Figure 9. Implementation of the proposed MLI (Source: developed by the authors)

3. Results

This section shows different results obtained by the testbed implementation. Four subsections are established to show different testbed results. The first three subsection shows preliminary results previous to the ECE15 reproduction.

In subsection 1, the MLI modulation results (SVM-NLC) are shown initially. Afterward, the fast response of the FOC is analyzed, getting the voltage and current response in front of high acceleration. An analysis of the mode transition of the PMSM between traction and generation is performed in subsection 3. Finally, the final section shows the EMS implementation.

1) SVM-NLC results: Figure 10 shows the modulation and vector selection employed. This graph was obtained when the PMSM had 1500 rpm (according to the I.M. limit). It is important to highlight different dv/dt occasioned by the voltage level transition. These voltage spikes are prevented using a Snubber Net in every IGBT occupied in the testbed. A fast Fourier transform FFT of the SVM-NLC modulation was performed in Fig. 11. Low harmonics are detected in this modulation kind. Consequently, it is possible to wait for reduced motor losses due to few harmonic signals. Figure 11 was determined using a velocity lower than 1500 rpm obtaining a fundamental signal of 60 Hz.

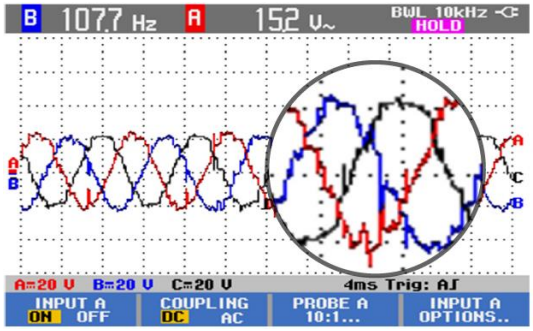

Figure 10. SVM-NLC Modulation (Source: developed by the authors)

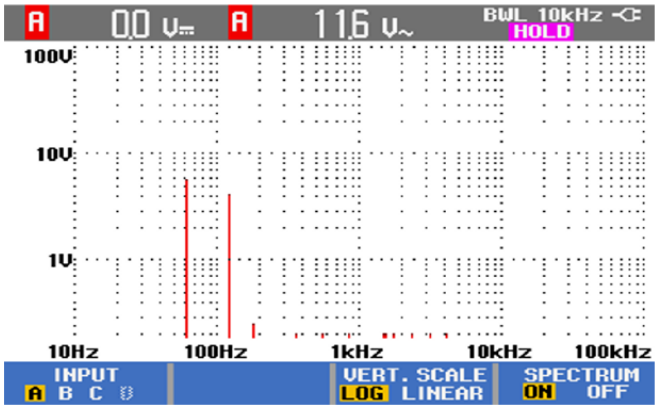

Figure 11. FFT for SVM-NLC (Source: developed by the authors)

2) SVM-NLC results: Figure 12 and Figure 13 show the back-EMF generated when the PMSM works as a generator. Meanwhile, Figure 12 shows the back-EMF at 1500 rpm. On the other side, Figure 13 gives the voltage and current generated at 800 rpm. This procedure verifies the generated power of the PMSM.

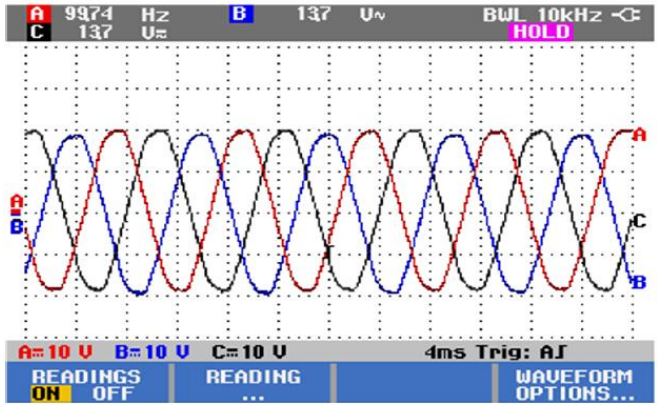

Figure 12. PMSM Back-EMF generated at 1500 rpm (Source: developed by the authors)

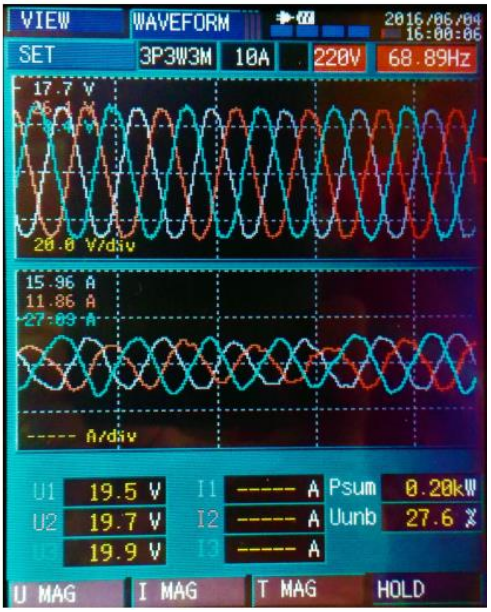

Figure 13. PMSM Back-EMF generated at 800 rpm obtained from a PQA (Source: developed by the authors)

3) FAST Dynamic of PMSM: This result shows the dynamic response of the PMSM in front of high acceleration. Figure 14 shows how the FOC modulates the voltage and frequency when the user requires a high acceleration. The FOC starts with a low voltage and frequency to overcome the motor inertia. The prototype quickly provides the current needed for fast acceleration of the PMSM, taking advantage of the high specific power of the ESS (composed of UCaps).

Figure 15 shows the motor current required to accelerate until 1500 rpm. As expected, the motor current is initially high; meanwhile, the inertia is overcome, and the current is reduced afterward.

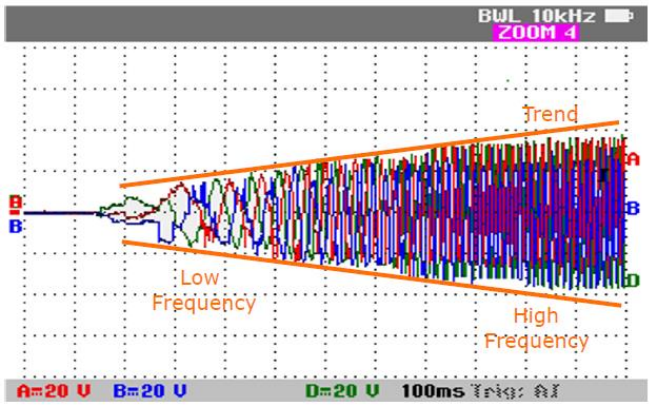

Figure 14. MLI voltage for fast acceleration (Source: developed by the authors)

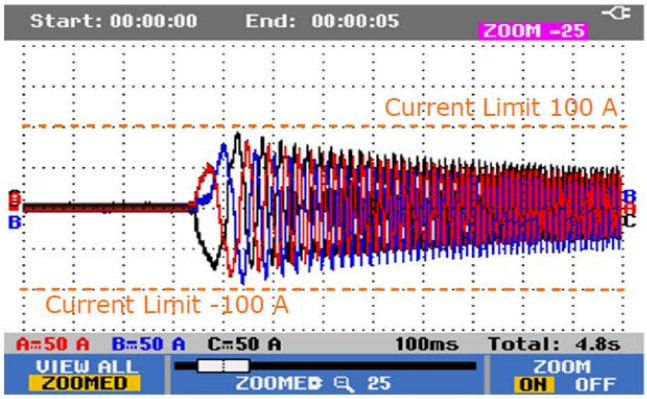

Figure 15. MLI current for fast acceleration (Source: developed by the authors)

4) Traction and Regenerative mode: Figure 16 was obtained with the motor's coupling and a constant load generated by the I.M. A visible transition between the traction mode and generator mode is shown in Figure 16.

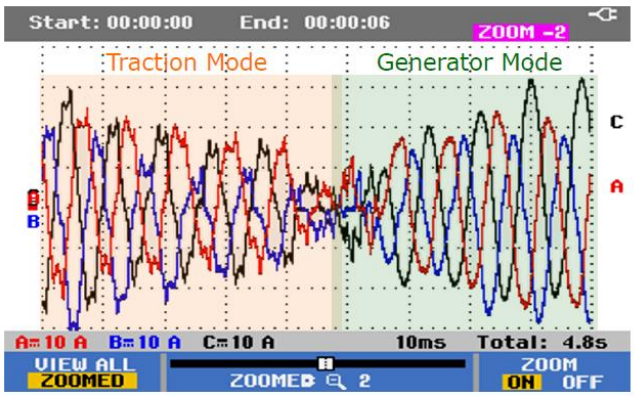

Figure 16. PMSM Transition between traction to generation (Source: developed by the authors)

5) Traction and Regenerative mode: The ECE15 cycle must be modified according to the revolutions restriction (1500 rpm) of the load I.M. for the test performance. Thus, all ECE15 speeds must be reduced. On the other hand, the ECE15 cycle should be followed manually by manipulating the Iq reference potentiometer (located in the testbed as shown in Figure 8). All speeds and times inside the cycle must have a tolerance band. An international standard for E.V. (ISO 8714) is used to reproduce the ECE15 driving cycle, as shown in Figure 17. The ISO 8714 standard is a test procedure for estimating the energy consumption and range for passenger and light commercial vehicles. The standard is predefined with a velocity tolerance of ±2 km/h and a time tolerance of ±1 s for the experimental reproduction of a driving cycle. As a standard advantage, the energy consumption has a low deviation from the accurate energy consumption.

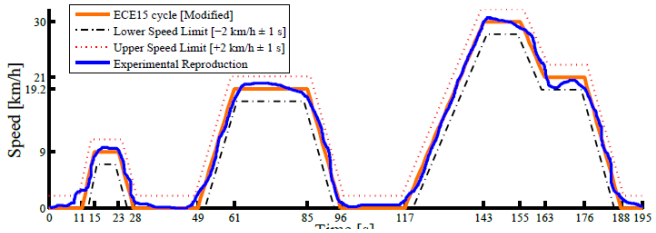

Figure 17. ECE15 experimental reproduction (Source: developed by the authors)

In the test, it should be noted that the prototype only handles a maximum of 100A (70.7 Arms) due to the technical constraints of IGBTs. For this reason, the maximum torque is obtained by multiplying the RMS current and the constant torque 0.14 engine Nm/A. As a result, the maximum torque generated by the PMSM under the current restrictions is 9.89 Nm, i.e., just 50 % of its 19.7 Nm of maximum torque.

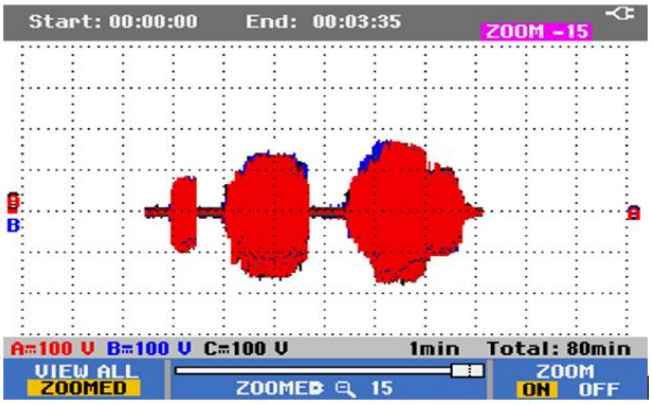

Figure 18. ECE15 Phase-phase voltage of the PMSM (Source: developed by the authors)

The ECE15 driving cycle used for testing the methodology is shown in Figure 18. As a result of the EMS control, Figure 18 was obtained. The UCap voltages present an adequate voltage balance between them. Additionally, the EMS controls pursue the reference with an error lower than 5%. As a result, the vehicle accurately follows the ECE15 driving cycle. Simultaneously, the FOC control works adequately, controlling the i_d and i_q currents controlling the SVPWM.

4. Discussion

The Energy Management System (EMS) tested using the Power Hardware-in-the-Loop (PHIL) setup shows that our multilevel inverter powered by ultracapacitors works very well in real-time conditions. The results indicate that the SVM-NLC modulation method is more efficient than the conventional SVPWM, reaching 91.7% compared to 90.6%. This improvement comes from fewer switching events, which reduce energy losses.

The system keeps the voltage ratio between the main and auxiliary ultracapacitor banks stable at 1:3, with errors under 5%. This precise control ensures smooth power delivery to the Permanent Magnet Synchronous Motor (PMSM), even during fast acceleration or regenerative braking. The predictive vector-selection strategy in SVM-NLC helps manage these rapid changes effectively.

The EMS also does a great job capturing energy during braking. It first stores energy in the main ultracapacitor and then sends extra energy to the auxiliary bank. This strategy maximizes recovery and reduces losses. Tests on the ECE15 driving cycle show the system can handle torque up to 9.89 Nm safely, even with the 100 A current limitation. Summary of Key Performance Metrics in shown in Table 5.

Overall, the results confirm that the EMS with SVM-NLC and the multilevel inverter:

- Improves inverter efficiency by reducing switching losses.
- Keeps ultracapacitor voltages well balanced.
- Recovers more energy during braking.
- Maintains accurate motor torque and current under dynamic conditions.
- Produces smooth currents, keeping THD low and system stable.
-

Table 5. Summary of Key Performance Metrics

Parameter	SVM-NLC	SVPWM	Unit	Notes
Inverter Efficiency	91.7	90.6	%	SVM-NLC reduces switching losses
Ultracapacitor Voltage Error	<5	<5	%	Maintains main:aux ratio 1:3
Maximum PMSM Torque	9.89	9.89	Nm	Limited by 100 A current
Motor Current THD	1.12	0.64	%	SVPWM slightly smoother
Energy Recovery Efficiency	95	92	%	Better regenerative braking with SVM-NLC
Switching Frequency	160	20,000	Hz	Lower in SVM-NLC, saving energy

In short, while SVPWM gives slightly smoother current, SVM-NLC improves efficiency and energy recovery, making it more practical for real-time EMS applications with ultracapacitors.

5. Conclusion

This paper introduced and tested an energy management system (EMS) for a multilevel inverter with total harmonic distortion (THD) below 10 percent, designed for electric powertrains in battery rapid transit systems. The authors employed Power Hardware-in-the-Loop (PHiL) methods to build and validate the system in a real-time testbed, ensuring effective inverter control and energy flow management. By harnessing the high-power density of ultracapacitors as the main energy source, the study optimized performance for real-world use.

The key contribution is the innovative, real-time PHiL implementation of an EMS in a flexible two-level multilevel inverter powered solely by ultracapacitors. This setup allows seamless two-way energy flow and stable voltage balancing via predictive vector selection with space vector modulation-nearest level control (SVM-NLC). In contrast to earlier research emphasizing simulations of hybrid systems or non-real-time optimizations, the hardware-verified approach delivers 91.71 percent efficiency under ECE15 driving cycles, extending vehicle range by up to 8.9 percent through reliable real-time control. These advancements pave the way for practical ultracapacitor-based powertrains that boost regenerative braking and minimize energy losses.

From the findings, the authors suggest incorporating this EMS into electric vehicle designs to improve energy recapture during braking and overall efficiency—especially in city transit where stops are common. Engineers may also favor SVM-NLC modulation over space vector pulse width modulation (SVPWM) when aiming for reduced switching losses and steady real-time operation.

Looking ahead, future work could examine hybrid setups blending ultracapacitors with batteries to prolong range and durability. Testing across varied driving scenarios, like highways or high-demand routes, and adapting the design for larger commercial vehicles would broaden its real-world potential. Exploring cutting-edge predictive tools or machine learning for smarter vector choices could further enhance flexibility in changing conditions.

Declarations

Author Contributions

Conceptualization, formal analysis and writing—review and editing Pereda-Torres J., Naranjo-Lourido W. and Martinez-Baquero J.; methodology, validation, investigation supervision, project administration, funding acquisition, and data curation Pereda-Torres J., Naranjo-Lourido W.; writing—original draft preparation and visualization Pereda-Torres J., Naranjo-Lourido W. All authors have read and agreed to the published version of the manuscript.

Data Availability Statement

The data presented in this project are available on request from the corresponding author.

Acknowledgements

The authors thank to Pontificia Universidad Catolica de Chile and Universidad de los Llanos for the time and support available for the development of this article where they are professors.

Informed Consent Statement

The study was developed with the prior signed consent of the participants

Conflicts of Interest

The author declares that there is no conflict of interests regarding the publication of this manuscript. In addition, the ethical issues, including plagiarism, informed consent, misconduct, data fabrication and/or falsification, double publication and/or submission, and redundancies have been completely observed by the authors.

References

[1] ZHANG B., YU Q., WU Y., WANG C. & MA, S. ISIGHT-Based Optimal Analysis of Torque Distribution in the Four-wheel Drive System of Electric Vehicles. IEEE 6th Information Technology and Mechatronics Engineering Conference (ITOEC), Chongqing, China, 2022, pp. 2031-2035. https://doi.org/10.1109/ITOEC53115.2022.9734676

[2] SIGLE S., EPPLE F. & SCHIER D.M. Investigation of the Applicability of a Two-Engine Concept for Electric Utility Vehicles, Fifteenth International Conference on Ecological Vehicles and Renewable Energies (EVER), MonteCarlo, Monaco, 2020, pp. 1-5. https://doi.org/10.1109/ever48776.2020.9242543

[3] SCHALL P., SIGLE S. & ULRICH C. Design Strategy for a Distributed Energy Storage in a Modular Mover. Sixteenth International Conference on Ecological Vehicles and Renewable Energies (EVER), Mónaco, 2021, pp 1-5. https://doi.org/10.1109/ever52347.2021.9456606

[4] AMJADI, Z. Energy Management of Fuel Cell/Battery & Ultra-capacitor Hybrid Energy Storage System for Electric Vehicle. IEEE Power & Energy Society Innovative Smart Grid Technologies Conference (ISGT), Washington, USA, 2020, pp. 1-5. https://doi.org/10.1109/ISGT45199.2020.9087635.

[5] SHI, S., ZHANG Y., NI L., YANG Q., FANG C., WANG H., WANG Y. & SHI, S. Energy management method for energy storage system in PV-integrated EV charging station. IEEE International Conference on Power Electronics, Computer Applications (ICPECA), Shenyang, China, 2021, pp.427-431. https://doi.org/10.1109/ICPECA51329.2021.9362623

[6] MS K., MOHAMMED S S. & PADMASURESH L. A Review on Optimal Energy Management Strategies for Electric Vehicles. Third International Conference on Intelligent Computing Instrumentation and Control Technologies (ICICICT). Kannur, India, 2022, pp. 1660-1663. https://doi.org/ 0.1109/ICICICT54557.2022.9917996

[7] SANDOVAL, M. & GRIJALVA, S. Electric vehicle-intelligent energy management system (EV-IEMS) for frequency regulation application. Transportation Electrification Conference and Expo (ITEC). Dearborn, MI, USA,2012,pp.1-6. https://doi.org/1 10.1109/ITEC.2012.6243510.

[8] YAVASOGLU H. A., SHEN J., SHI C., GOKASAN M. & KHALIGH A. Power Split Control Strategy for an EV Powertrain With Two Propulsion Machines. *IEEE Transactions on Transportation Electrification*, 2015,1(4): pp. 382-390. https://doi.org/1 0.1109/TTE.2015.2437338

[9] ELDEEB H., ELSAYED A.T., LASHWAY C.R. & MOHAMMED O. Hybrid Energy Storage Sizing and Power Splitting Optimization for Plug-in Electric Vehicles. IEEE Industry Applications Society Annual Meeting (IAS), Portland, OR, USA, 2018, pp. 1-8. https://doi.org/ 10.1109/IAS.2018.8544674.
[10] ELDEEB H., ELSAYED A.T., LASHWAY C.R. & MOHAMMED O. Hybrid Energy Storage Sizing and Power Splitting Optimization for Plug-in Electric Vehicles. *IEEE Transactions on Industry Applications*, 2019,55(3): pp. 2252-2262. https://doi.org/ 10.1109/TIA.2019.2898839.
[11] WANG S.C., YANG J., ZHENG Y.F., GUAN Q.Y., HUANG J.Q., SANG Z.H., CHENG Z. & LEI H. Genetic Algorithm Based Optimal Strategy for Smart Home Energy Management System with Solar Power and Electric Vehicles. 4th International Conference on Mechanical, Control and Computer Engineering (ICMCCE), Hohhot, China, 2019, pp. 979-993.
https://doi.org/10.1109/ICMCCE48743.2019.00220.
[12] BHATTACHARYYA P., BANERJEE A., SEN S., GIRI S. K., AND SADHUKHAN S. A Modified Semi-Active Topology for Battery-Ultracapacitor Hybrid Energy Storage System for EV Applications. IEEE International Conference on Power Electronics, Smart Grid and Renewable Energy (PESGRE2020), Cochin, India, 2020, pp. 1-6. https://doi.org/ 10.1109/PESGRE45664.2020.9070531
[13] Guo L., Yang B. & Ye J. Predictive Energy Management for Dual-Motor BEVs Considering Temperature-Dependent Traction Inverter Loss,in *IEEE Transactions on Transportation Electrification*,2022,8(1): pp. 1501-1515. https://doi.org/ 10.1109/TTE.2021.3116883
[14] RATHORE V., RAJASHEKARA K., NAYAK P. & RAY A. A High-Gain Multilevel dc–dc Converter for Interfacing Electric Vehicle Battery and Inverter. *IEEE Transactions on Industry Applications*, 2022,58(5): pp. 6506-6518.
https://doi.org/ 10.1109/TIA.2022.3185183
[15] SHEIR A., YOUSSEF M.Z. & ORABI M. A Novel Bidirectional T-Type Multilevel Inverter for Electric Vehicle Applications. *IEEE Transactions on Power Electronic, 2019,* 34(7):pp.6648-6658.
https://doi.org/10.1109/TPEL.2018.2871624.
[16] Mukherjee S., Giri S. K. & Banerjee S. A Flexible Discontinuous Modulation Scheme With Hybrid Capacitor Voltage Balancing Strategy for Three-Level NPC Traction Inverter. *IEEE Transactions on Industrial Electronics*, 2019,66,(5):pp3333-3343.
https://doi.org/10.1016/j.matpr.2020.06.553.
[17] DHANAMJAYULU C., PADMANABAN S., RAMACHANDARAMURTHY V.K., HOLM-NIELSEN J.B. & BLAABJERG F. Design and Implementation of Multilevel Inverters for Electric Vehicles. *IEEE Access*, 2021, 9: pp. 317-338.
https://doi.org/ 10.1109/ACCESS.2020.3046493.
[18] NARANJO W., PEREDA, J., MUÑOZ, L. E. & CORTES, C. Energy evaluation of different inverter topologies and modulations used on electric vehicles. Industrial Electronics Society. IECON 2015 - 41st Annual Conference of the IEEE, Yokohama, 2015, 002142-002147. https://doi.org/ 10.1109/IECON.2015.7392418

参考文:

[1] ZHANG B., YU Q., WU Y., WANG C. & MA, S. 基於ISIGHT的電動車四輪驅動系統扭矩分配最優分析。IEEE第六屆資訊技術與機電工程會議（ITOEC），中國重慶, 2022, pp. 2031-2035. https://doi.org/10.1109/ITOEC53115.2022.9734676
[2] SIGLE S., EPPLE F. & SCHIER D.M. 雙引擎概念在電動公用事業車輛適用性之研究第十五屆生態車輛與再生能源國際會議（EVER）蒙地卡羅，摩納哥, 2020, pp. 1-5. https://doi.org/10.1109/ever48776.2020.9242543
[3] SCHALL P., SIGLE S. & ULRICH C. 模組化移動裝置中分散式能源儲存系統之設計策略第十六屆生態車輛與再生能源國際會議（EVER）摩納哥, 2021, pp 1-5. https://doi.org/10.1109/ever52347.2021.9456606
[4] AMJADI, Z. 電動車用燃料電池/電池與超級電容器混合儲能系統之能源管理。IEEE電力與能源學會創新智慧電網技術會議（ISGT），美國華盛頓, 2020, pp. 1-5. https://doi.org/10.1109/ISGT45199.2020.9087635.
[5] SHI, S., ZHANG Y., NI L., YANG Q., FANG C., WANG H., WANG Y. & SHI, S. 光伏整合式電動車充電站儲能系統之能源管理方法。IEEE國際電力電子與電腦應用會議（ICPECA），中國瀋陽，2021, pp.427-431. https://doi.org/10.1109/ICPECA51329.2021.9362623
[6] MS K., MOHAMMED S S. & PADMASURESH L. 電動車最佳能源管理策略綜述。第三屆國際智能計算儀器與控制技術會議（ICICICT）。印度坎努爾。 2022, pp. 1660-1663. https://doi.org/ 0.1109/ICICICT54557.2022.9917996
[7] SANDOVAL, M. & GRIJALVA, S. 電動車智能能源管理系統（EV-IEMS）之頻率調節應用。交通電氣化會議暨博覽會（ITEC）。美國密西根州迪爾伯恩市,2012,pp.1-6.
https://doi.org/1 10.1109/ITEC.2012.6243510.
[8] YAVASOGLU H. A., SHEN J., SHI C., GOKASAN M. & KHALIGH A. 雙推進機電動車動力系統的功率分配控制策略。IEEE 交通電氣化交易會, 2015,1(4): pp. 382-390. https://doi.org/1 0.1109/TTE.2015.2437338
[9] ELDEEB H., ELSAYED A.T., LASHWAY C.R. & MOHAMMED O. 插電式電動車混合能源儲存系統容量配置與功率分配優化。IEEE工業應用學會年會（IAS），美國俄勒岡州波特蘭市, 2018, pp. 1-8. https://doi.org/ 10.1109/IAS.2018.8544674.
[10] ELDEEB H., ELSAYED A.T., LASHWAY C.R. & MOHAMMED O. 插電式電動車混合能源儲存系統容量配置與功率分配優化。IEEE工業應用彙刊, 2019,55(3): pp. 2252-2262. https://doi.org/ 10.1109/TIA.2019.2898839.
2262. https://doi.org/ 10.1109/TIA.2019.2898839.
[11] WANG S.C., YANG J., ZHENG Y.F., GUAN Q.Y., HUANG J.Q., SANG Z.H., CHENG Z. & LEI H. 基於遺傳演算法的太陽能與電動車智慧家庭能源管理系統最優策略。第四屆國際機械、控制與電腦工程會議（ICMCCE），中國呼和浩特，2019, pp. 979-993. https://doi.org/10.1109/ICMCCE48743.2019.00220.
[12] BHATTACHARYYA P., BANERJEE A., SEN S., GIRI S. K., AND SADHUKHAN S. 適用於電動車應用的電池-超級電容器混合儲能系統之改良型半主動拓撲結構。IEEE國際電力電子、智慧電網與再生能源會議（PESGRE2020），印度科欽, 2020, pp. 1-6. https://doi.org/ 10.1109/PESGRE45664.2020.9070531

[13] GUO L., YANG B. & YE J. 考慮溫度依賴性牽引逆變器損耗的雙馬達純電動車預測性能源管理，發表於《IEEE 交通電氣化交易》期刊,2022,8(1): pp. 1501-1515. https://doi.org/ 10.1109/TTE.2021.3116883
[14] RATHORE V., RAJASHEKARA K., NAYAK P. & RAY A. 高增益多級直流-直流轉換器：用於電動車電池與逆變器之介面連接。IEEE工業應用彙刊, 2022,58(5): pp. 6506-6518.
https://doi.org/ 10.1109/TIA.2022.3185183
[15] SHEIR A., YOUSSEF M.Z. & ORABI M. 一種新型雙向T型多層次逆變器在電動車輛中的應用。IEEE電力電子學報, *2019,* 34(7):pp.6648-6658.
https://doi.org/10.1109/TPEL.2018.2871624.
[16] MUKHERJEE S., GIRI S. K. & BANERJEE S. 一種具備混合電容器電壓平衡策略的靈活不連續調變方案，適用於三級非同步可控樞器牽引逆變器。IEEE工業電子學彙刊,2019,66,(5):pp3333-3343. https://doi.org/10.1016/j.matpr.2020.06.553.
[17] DHANAMJAYULU C., PADMANABAN S., RAMACHANDARAMURTHY V.K., HOLM-NIELSEN J.B. & BLAABJERG F. 電動車多層次逆變器的設計與實現。IEEE Access, 2021, 9: pp. 317-338.
https://doi.org/ 10.1109/ACCESS.2020.3046493.
[18] NARANJO W., PEREDA, J., MUÑOZ, L. E. & CORTES, C. 不同逆变器拓扑结构与调制方式在电动汽车中的能量评估。工业电子学会。IECON 2015 - 第41届IEEE 年度会议，横滨，2015, 002142-002147. https://doi.org/ 10.1109/IECON.2015.7392418

Manuscript Information
Word count: 7,783 words (excluding references).

Peer-Review Record
Fast-track status: Not fast-tracked.
First-round reviews received: 3 reports.
Revision cycles completed: 3 rounds.
Final version submitted: December 11, 2025